

# Hybrid Predictive Quantum Feedback: Extending Qubit Lifetimes Beyond the Wiseman-Milburn Limit

Ali Abu-Nada\* Aryan Iliat† Russell Ceballos‡§

\*Sharjah Maritime Academy, Sharjah, United Arab Emirates

Email: ali.abunada@sma.ac.ae

†School of Physics and Applied Physics, Southern Illinois University, Carbondale, IL 62903, USA

Email: aryan.iliat@siu.edu

‡Department of Physical Sciences, Olive-Harvey College, City Colleges of Chicago, 10001 S Woodlawn Ave, Chicago, IL 60628, USA

§QuSTEAM Initiative, 510 Ronalds St., Iowa City, IA 52245, USA

**Abstract**—Amplitude damping fundamentally limits qubit lifetimes by irreversibly leaking energy and information into the environment. Standard Wiseman–Milburn feedback [1] offers only modest improvement because it acts on a single measured quadrature and its corrective drive is degraded by loop delay. We introduce a compact hybrid upgrade with two components: (i) a coherently coupled *ancilla* qubit that receives the homodyne current and feeds back *quantum-coherently* on the system, recovering information from *both* field quadratures and intentionally engineered to decay much faster than the system; and (ii) a lightweight supervised predictor that forecasts the near-future homodyne current, phase-aligning the correction to overcome hardware latency. A Lindblad treatment yields closed-form effective decay rates: the ancilla suppresses the emission channel by a cooperativity factor, while the predictor further suppresses the residual decay in proportion to forecast quality. Using IBM-scale parameters (baseline  $T_1 = 50 \mu\text{s}$ ), numerical simulations surpass the W–M limit, achieving  $\sim 3\text{--}4\times$  longer  $T_1$  together with improved population retention and integrated energy. The method is modular and hardware-compatible: ancilla coupling and supervised prediction can be added to existing W–M loops to convert leaked information into a precise, time-advanced corrective drive. We also include a detailed, student-friendly derivation of the effective rates for both ancilla-assisted and prediction-enhanced feedback, making the impact of each design element analytically transparent.

## I. INTRODUCTION

The loss of energy from a quantum system to its environment, known as *amplitude damping*, is one of the main causes of decoherence in quantum technology. When an excited qubit emits a photon and falls to its ground state, the superposition needed for quantum computation, communication, and sensing is destroyed [2], [3]. The timescale of this process, the relaxation time  $T_1$ , therefore places a strict limit on qubit performance: a larger  $T_1$  means higher-fidelity gates and less overhead in quantum error correction [4]–[6].

Two main approaches are commonly used to extend  $T_1$ . The first is *environment engineering*, which reduces the electromagnetic density of states at the qubit frequency, since

$T_1^{-1} \propto S_{\perp}(\omega_0)$ . Examples include Purcell filters [7]–[12] and photonic bandgap structures [13], [14]. Although effective, these require precise fabrication and careful frequency matching. The second approach is *active control*. Dynamical decoupling (DD) can refocus low-frequency phase noise [15]–[23], but offers little protection against amplitude damping, which is driven by high-frequency fluctuations near  $\omega_0$  [18], [24]–[27].

A different idea was introduced by Wiseman and Milburn [28]–[30]. Instead of modifying the environment or applying predetermined pulses, their framework uses *continuous measurement and feedback*. The field emitted by the qubit is monitored in real time, usually by homodyne detection, producing a measurement signal. This signal is immediately fed back as a control operation. In this way, the measurement itself becomes part of the dynamics and can slow down the decay [1]. Figure 1 shows the basic W–M feedback circuit. A laser is tuned to the qubit transition frequency  $\omega_0$ , the natural energy splitting between  $|e\rangle$  and  $|g\rangle$ . The laser is split into two paths. One path, labeled  $\beta$ , is sent directly to the detectors and serves as the strong local oscillator (LO) needed for homodyne detection. The other path, labeled  $\alpha$ , drives the qubit. This probe field is later modulated by the feedback as  $\alpha + \lambda I(t)$ . The qubit emits a weak field at the same frequency  $\omega_0$ . This weak emission and the strong LO interfere on a 50:50 beam splitter, and the two output ports are measured by detectors D1 and D2, producing photocurrents  $i_1(t)$  and  $i_2(t)$ .

To understand what the detectors measure, recall that the qubit’s emitted field can be written in terms of two independent components, called quadratures,  $\hat{E}_{\text{field}}(t) = \hat{E}_x(t) \cos(\omega_0 t) + \hat{E}_y(t) \sin(\omega_0 t)$ , where  $\hat{E}_x$  is the in-phase part and  $\hat{E}_y$  is the out-of-phase part. For a two-level system, these quadratures correspond to the Pauli operators,  $\hat{E}_x \propto \sigma_x^{(S)}$  and  $\hat{E}_y \propto \sigma_y^{(S)}$ . The LO field  $E_{\text{LO}}(t) = E_0 \cos(\omega_0 t + \phi)$  provides a stable phase reference. When the LO and emitted field meet at the beam splitter, each detector measures a large intensity

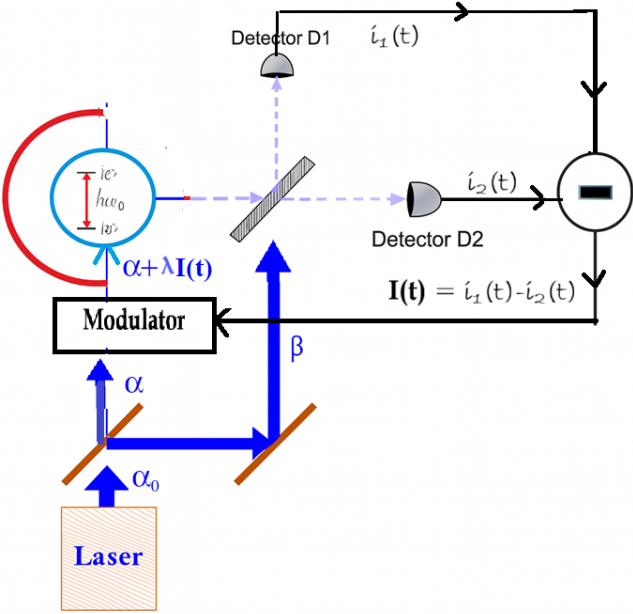


Fig. 1. Schematic of the feedback-controlled homodyne interferometer used to monitor and stabilize the emission of a two-level system with transition frequency  $\omega_0$ . A coherent laser drive is split into a probe arm ( $\alpha_0 \rightarrow \alpha$ ) and a reference arm ( $\beta$ ). The emitter's scattered field is combined with the reference on a 50:50 beam splitter and measured on two photodetectors (D1, D2), producing photocurrents  $i_1(t)$  and  $i_2(t)$ . Their difference  $I(t) = i_1(t) - i_2(t)$  is fed back through a modulator to adjust the drive amplitude  $\alpha + \lambda I(t)$ , enabling real-time stabilization/noise control of the emitter dynamics.

dominated by the LO, so neither  $i_1(t)$  nor  $i_2(t)$  alone carries clear information about the qubit.

The key step is to subtract the detector outputs,  $I(t) = i_1(t) - i_2(t)$ , which removes the large DC background from the LO and leaves only the small interference term between the LO and the qubit emission. In the strong-LO limit, this interference is proportional to a chosen quadrature,  $I(t) \propto E_0 [\hat{E}_x(t) \cos \phi + \hat{E}_y(t) \sin \phi] \propto \langle \sigma_\phi^{(S)} \rangle$ , where  $\sigma_\phi^{(S)} = \sigma_x^{(S)} \cos \phi + \sigma_y^{(S)} \sin \phi$ . Thus, by selecting the LO phase  $\phi$ , the detector measures either  $\sigma_x$  (in-phase) or  $\sigma_y$  (out-of-phase). This gives a clean, amplified measurement of one quadrature of the qubit's emission. The homodyne current is usually written as  $I(t) = \sqrt{\eta\gamma} \langle \sigma_\phi \rangle_c(t) + \frac{\xi(t)}{\sqrt{\eta}}$ , where  $\eta$  is the detector efficiency,  $\gamma$  is the spontaneous emission rate,  $\langle \sigma_\phi \rangle_c(t)$  is the measured quadrature, and  $\xi(t)$  is the measurement noise.

This current is fed back to modulate the drive field as  $\alpha + \lambda I(t)$ , so that the correction field interferes with the qubit's emitted field and partially cancels it, slowing the decay. However, the W-M method has two fixed limitations that cannot be avoided by simply improving the hardware. First, homodyne detection measures only *one* quadrature of the emitted field. This means the feedback knows only half of what the qubit is doing. It can push the qubit back along one direction of the Bloch sphere, but the motion along the unmeasured direction is completely invisible and therefore cannot be corrected. As a result, part of the spontaneous emission always escapes, and

the lifetime improvement is limited to  $T_1^{\text{eff}} \leq 2T_1$ . Second, real experiments have a small but unavoidable electronic delay. Because the qubit evolves very fast, even a few nanoseconds of delay causes the correction to arrive with the wrong phase, making it much less effective and sometimes even harmful. These two issues, missing information and delayed correction, motivate our hybrid predictive feedback strategy.

**Step 1: Add an ancilla qubit (to recover the missing quadrature).** We introduce a second qubit that is coherently coupled to the main system qubit. The feedback signal  $I(t)$  does not drive the system directly; it drives the ancilla. As the ancilla precesses under its Hamiltonian, its motion naturally mixes the  $x$  and  $y$  components of its Bloch vector. Through the coherent coupling between system and ancilla, this mixed motion acts back on the system and generates a correction that has *both* quadratures. In this sense, the ancilla behaves like a quantum “translator”: it takes the one-dimensional classical measurement signal and turns it into a full two-dimensional quantum correction. This allows the feedback to act along both directions of the Bloch sphere, overcoming the single-quadrature restriction of the W-M method. **Step 2: Predict the future (to fix the delay).** The second limitation of the W-M scheme is hardware delay: cables and electronics introduce a small delay  $\tau$ , so using the measured current  $I(t)$  directly means the correction always arrives slightly too late. By the time the feedback reaches the qubit, the qubit's state has already changed, and the correction is applied with the wrong phase. To overcome this, we train a supervised machine-learning model to predict the future homodyne signal,  $\hat{I}(t+\tau)$ , from the recent history of the measurement record. As shown in Fig. 4, the predicted current (blue curve) closely matches the true future current  $I(t+\tau)$  (red curve), while the present signal  $I(t)$  (dashed gray) is clearly out of sync. By using the predicted future value instead of the delayed measurement, the feedback arrives *in phase* with the qubit's emission, restoring the destructive interference needed for strong suppression of spontaneous decay.

Figure 2 shows the full hybrid loop. The emitted field is measured, converted into the homodyne current, and then predicted forward in time by the ML model. This predicted current drives the modulator, which updates the probe field. The corrected drive interacts with the ancilla, which applies a fast, coherent, two-quadrature correction to the system. Together, the ancilla and the predictor suppress spontaneous emission *as it happens*, achieving much stronger stabilization than the classical W-M loop.

## II. FROM CLASSICAL FEEDBACK TO HYBRID PREDICTIVE QUANTUM CONTROL

Real-time feedback has long been used to stabilize or cool quantum systems, but conventional W-M feedback remains limited by two fundamental constraints: (i) it acts only on a single field quadrature, so half of the available information is lost to the environment, and (ii) it operates with a finite delay  $\tau$  between measurement and control, so the corrective tone always arrives *after* the emission it seeks to cancel. These

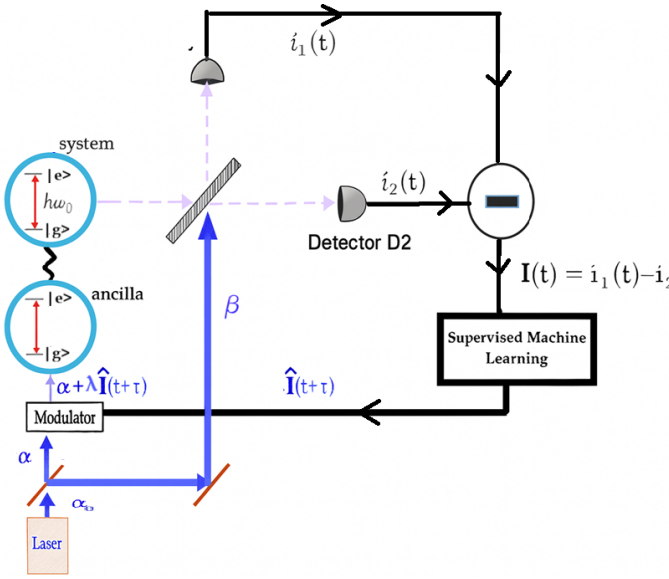


Fig. 2. **Hybrid predictive feedback scheme.** The emitted light from the system is measured by two detectors (D1, D2), producing the homodyne current  $I(t) = i_1(t) - i_2(t)$ . A supervised machine-learning model predicts the future signal  $\hat{I}(t+\tau)$  to overcome the feedback delay  $\tau$ . The predicted current drives the modulator, which adjusts the laser field to  $\alpha + \lambda\hat{I}(t+\tau)$ . This corrected field interacts with a coherently coupled *ancilla* qubit, which then steers the main system qubit. Together, the ancilla and the ML predictor allow the feedback to act on both field quadratures and stay in phase with the emission, achieving stronger suppression of spontaneous decay than the standard W-M loop.

restrictions impose a hard twofold ceiling on the achievable lifetime extension ( $T_1^{\text{eff}} \leq 2T_1$ ).

To overcome these limits, we introduce a hybrid architecture that combines a *quantum-coherent ancilla* with a *supervised machine-learning predictor*. The ancilla couples coherently to the system, allowing the feedback to act simultaneously on both field quadratures and thus recover the half of the information lost in W-M control. Meanwhile, the machine-learning predictor forecasts the future homodyne current  $\hat{I}(t+\tau)$ , enabling phase-aligned actuation that compensates the physical propagation delay in the loop. Together, these upgrades convert classical measurement-based feedback into a fully predictive quantum-control protocol capable of surpassing the W-M lifetime limit. The following subsections describe these two components in detail.

#### A. Effective Dynamics of Ancilla-Assisted Feedback

In the original W-M scheme [1], [28], [29], a decaying qubit emits light that, like any electromagnetic wave, contains two orthogonal *quadratures*: an in-phase ( $x$ ) component and an out-of-phase ( $y$ ) component. Balanced homodyne detection (Fig. 1) mixes this weak field with a strong local oscillator (LO) of phase  $\phi$  and measures only *one* quadrature at a time. The two photodetectors produce a single classical signal, the homodyne current,  $I(t) \propto \langle \sigma_{\phi}^{(S)} \rangle_c(t)$ ,  $\phi = 0$  ( $x$ ),  $\phi = \frac{\pi}{2}$  ( $y$ ). Because  $I(t)$  contains information from only one quadrature, the feedback loop can push back only along one

direction of the Bloch sphere and therefore cannot fully cancel spontaneous emission.

*A quantum helper (ancilla) to recover the missing quadrature.:* To overcome this limitation, we introduce a second qubit, the *ancilla*, and let the measured current drive the ancilla instead of the system (Fig. 2). The ancilla is *coherently* coupled to the system, so the feedback now enters the loop at the quantum level. This allows the loop to affect *both* quadratures of the system's motion. Intuitively, the ancilla acts as a “quantum translator”: even though  $I(t)$  carries only one quadrature, the ancilla's own coherent evolution mixes its  $x$  and  $y$  components and converts the one-dimensional classical signal into a phase-aware two-quadrature correction on the system.

*Conditional stochastic evolution.:* Let  $\rho_{SA,c}$  be the conditional state of the system (S) and ancilla (A). Under continuous homodyne monitoring, it evolves according to [29], [31], [32]

$$d\rho_{SA,c} = -\frac{i}{\hbar} [H_0 + H_{\text{int}}, \rho_{SA,c}] dt + \gamma \mathcal{D} \left[ \sigma_{-}^{(S)} \right] \rho_{SA,c} dt + \sqrt{\eta\gamma} \mathcal{H} \left[ \sigma_{-}^{(S)} \right] \rho_{SA,c} dW(t), \quad (1)$$

where  $\gamma$  is the spontaneous-emission rate,  $\eta$  is the detector efficiency, and  $dW(t)$  is a Wiener increment ( $\mathbb{E}[dW] = 0$ ,  $dW^2 = dt$ ). The dissipator  $\mathcal{D}$  describes decay and  $\mathcal{H}$  describes measurement back-action.

#### Hamiltonians and coherent coupling.:

$$H_0 = H_S + H_A + H_{\text{drive}}^{(A)}(t), \quad H_S = \frac{\hbar\omega_S}{2} \sigma_z^{(S)}, \quad H_A = \frac{\hbar\omega_A}{2} \sigma_z^{(A)}, \quad (2)$$

$$H_{\text{int}} = \hbar g \left( \sigma_x^{(S)} \sigma_x^{(A)} + \sigma_y^{(S)} \sigma_y^{(A)} \right),$$

where  $H_S$  and  $H_A$  are the system and ancilla Hamiltonians,  $\omega_S$  and  $\omega_A$  are their transition frequencies, and  $g$  is the coherent coupling rate.

*Feedback acts on the ancilla.:* The feedback signal controls the ancilla:

$$H_{\text{drive}}^{(A)}(t) = \hbar u(t) \sigma_q^{(A)}, \quad u(t) = \lambda I(t), \quad q \in \{x, y\}, \quad (3)$$

with gain  $\lambda$  and axis  $q$  set by the LO phase. The homodyne current takes the explicit form

$$I(t) = \sqrt{\eta\gamma} \langle \sigma_{\phi}^{(S)} \rangle_c(t) + \frac{\xi(t)}{\sqrt{\eta}}, \quad (4)$$

where  $\xi(t)$  is white shot noise. Thus the ancilla is driven by a signal that originates entirely from the system's emission.

*How one quadrature becomes two.:* Although the drive  $u(t)$  pushes the ancilla along one axis (say,  $x$ ), the ancilla precesses under its Hamiltonian  $H_A = (\hbar\omega_A/2)\sigma_z^{(A)}$ . This rotation mixes its  $x$  and  $y$  components:

$$\sigma_x^{(A)}(t) = \cos(\omega_A t) \sigma_x^{(A)} + \sin(\omega_A t) \sigma_y^{(A)}. \quad (5)$$

Through  $H_{\text{int}}$ , these mixed quadratures couple back into the system's  $\sigma_x^{(S)}$  and  $\sigma_y^{(S)}$  operators, effectively generating a two-quadrature correction. The ancilla therefore acts as a *quantum*

converter: it transforms a single-number classical signal into a coherent, phase-aware control action that addresses both quadratures.

*Averaged (deterministic) dynamics.*: Averaging Eq. (1) over the measurement noise gives the unconditional Lindblad evolution

$$\dot{\rho}_{SA} = -\frac{i}{\hbar} \left[ H_0 + H_{\text{int}} + \frac{\hbar}{2} (c^\dagger \hat{\Lambda} + \hat{\Lambda} c), \rho_{SA} \right] + \mathcal{D}[c - i\hat{\Lambda}] \rho_{SA} + (1 - \eta) \mathcal{D}[\hat{\Lambda}] \rho_{SA}, \quad (6)$$

where  $c = \sqrt{\gamma} \sigma_-^{(S)}$  is the system emission operator and  $\hat{\Lambda} = \lambda \sigma_q^{(A)}$  is the ancilla feedback operator. The coherent term produces Hamiltonian shifts due to feedback, while the dissipators show explicitly how the ancilla's radiation destructively interferes with the system's emission, reducing the effective decay rate. Setting  $\hat{\Lambda} = \lambda \sigma_q^{(S)}$  recovers the classical W-M master equation [1], confirming that our approach is a *quantum-coherent generalization* of W-M feedback.

In Sec. II-B we extend this model by driving the ancilla with a short-horizon *prediction* of the homodyne current rather than the measured value itself,  $u(t) = \lambda \hat{I}(t + \tau)$ , where  $\hat{I}(t + \tau)$  is a supervised ML estimate of the future signal. This keeps the feedback phase-aligned despite electronic delay and further strengthens the suppression of spontaneous emission.

### B. Supervised Machine-Learning Prediction of the Homodyne Current

In the feedback setup, the balanced homodyne detector continuously measures the quadrature of the emitted field and produces an analog voltage signal  $I(t)$ . This signal fluctuates because of quantum noise, yet it carries valuable information about the instantaneous system state. In any real experimental setup, there exists a finite electronic latency  $\tau$ , arising from cables, filters, and data-processing circuits. As a result, a control signal calculated at time  $t$  will only reach the ancilla and influence the system at time  $t + \tau$ . If feedback were based solely on the instantaneous value  $I(t)$ , it would arrive too late to counteract the system's evolution. To overcome this, we train a supervised machine-learning (ML) model to *predict the future current  $I(t + \tau)$*  from the recent measurement history. The predicted signal is then used to drive the ancilla with a phase-leading control tone, so that, after the loop delay, it arrives synchronized with the actual optical field.

The experiment proceeds in two distinct stages: a *training stage* and a *prediction stage*.

During Stage 1 (Training), the ancilla feedback path is temporarily disconnected, and a probe device is placed at the ancilla input port to record the homodyne signal *after the loop delay*. This produces a delayed record  $\{I(t_0 + \tau), I(t_1 + \tau), I(t_2 + \tau), \dots\}$  sampled at regular intervals  $\Delta t = \tau$ , so that consecutive times differ by one loop delay:  $t_{i+1} - t_i = \tau$ . From this delayed record, the training dataset is constructed by sliding a window of width  $W = 5$ , as shown in Fig 3 and summarized in Table I.

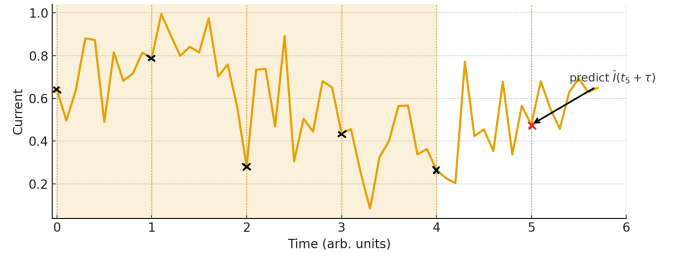


Fig. 3. **Digitizing the homodyne signal and forming training samples.** The orange curve shows the measured homodyne current  $I(t)$  after analog-to-digital conversion. Each black cross marks one of the five most recent samples  $[I(t_{i-5}), \dots, I(t_{i-1})]$  that form the input vector  $\mathbf{x}_i$ , while the red point represents the next sample  $I(t_i)$ , which the network learns to predict. This sliding-window process converts the continuous signal into overlapping input-output pairs suitable for supervised learning.

TABLE I  
TRAINING PAIRS CONSTRUCTED FROM THE DELAYED RECORD. THE SAMPLING STEP IS FIXED AT  $\Delta t = \tau$ , SO EACH ENTRY IN THE INPUT WINDOW IS EXACTLY ONE DELAY INTERVAL APART.

Input window $\mathbf{x}_i$	Target $y_i$
$[I(t_0 + \tau), I(t_1 + \tau), I(t_2 + \tau), I(t_3 + \tau), I(t_4 + \tau)]$	$I(t_5 + \tau)$
$[I(t_1 + \tau), I(t_2 + \tau), I(t_3 + \tau), I(t_4 + \tau), I(t_5 + \tau)]$	$I(t_6 + \tau)$
$[I(t_2 + \tau), I(t_3 + \tau), I(t_4 + \tau), I(t_5 + \tau), I(t_6 + \tau)]$	$I(t_7 + \tau)$
$\vdots$	$\vdots$

Each training example consists of five consecutive delayed samples as the input window and the next delayed sample as the target:

$$\begin{aligned} \mathbf{x}_i &= [I(t_{i-5} + \tau), I(t_{i-4} + \tau), I(t_{i-3} + \tau), I(t_{i-2} + \tau), \\ &\quad I(t_{i-1} + \tau)], \\ y_i &= I(t_i + \tau). \end{aligned} \quad (7)$$

When the network is trained properly, its predicted value for a representative window, such as the first row of Table I, satisfies  $\hat{I}(t_5 + \tau) \approx I(t_5 + \tau)$ , and the mean squared error (MSE) over all samples becomes sufficiently small. As will be explained in the next subsection, this MSE serves as the quantitative measure of training success. *Once the model has been trained to predict the next delayed sample accurately, the probe is removed and the ancilla is reconnected to begin live feedback operation.*

During Stage 2 (Live prediction), the ML continuously receives the most recent five delayed samples  $[I(t_{i-5} + \tau), \dots, I(t_{i-1} + \tau)]$ , feeds them to the trained model, and obtains a real-time prediction for the next delayed value  $\hat{I}(t_i + \tau)$ . This forecast is used immediately to generate the control drive  $u(t) = \lambda \hat{I}(t + \tau)$ , so that, after the delay  $\tau$ , the control signal arrives phase-aligned with the true homodyne current.

After we train the network offline on the recorded delayed data, we run it online in real time: at each step it predicts  $\hat{I}(t + \tau)$  from the latest five samples and the controller applies

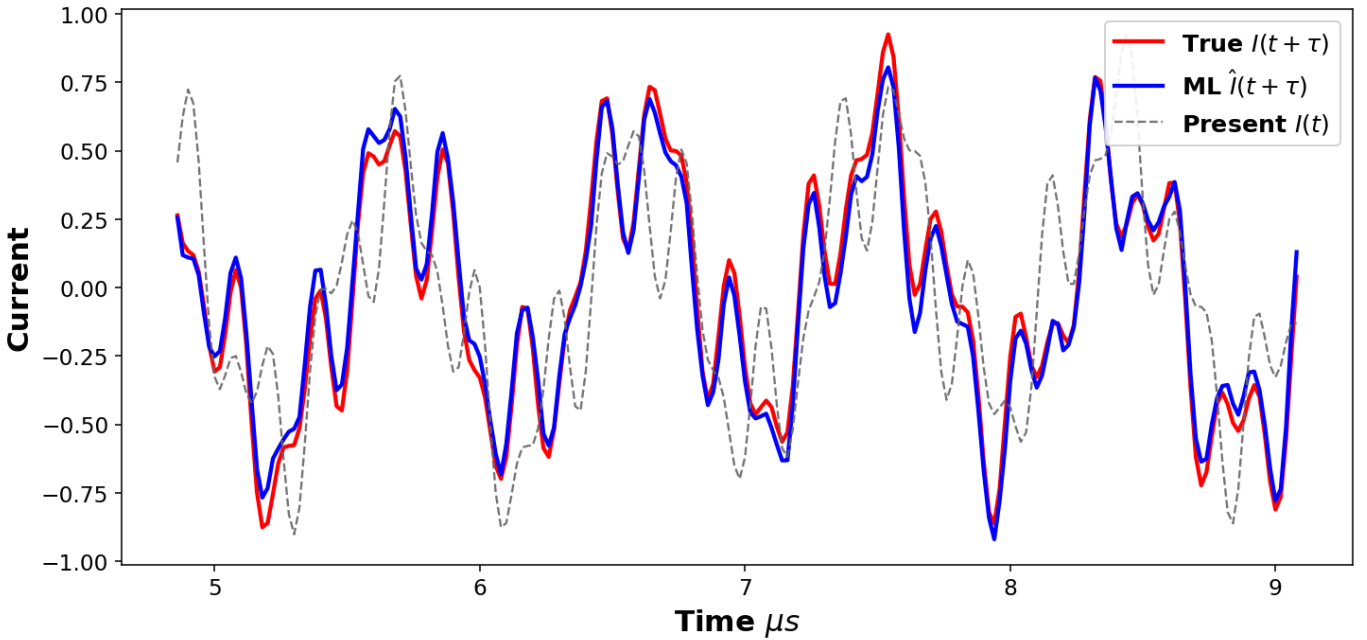


Fig. 4. **Prediction versus measured delayed current.** The red curve shows the measured delayed current  $I(t+\tau)$ , while the blue curve shows the ML prediction  $\hat{I}(t+\tau)$  obtained from the input windows in Table I. The dashed gray curve indicates the present current  $I(t)$ . The close overlap between red and blue confirms that the trained network accurately anticipates the future signal, allowing the feedback to stay synchronized despite the hardware latency.

$u(t) = \lambda \hat{I}(t+\tau)$ . This turns a delayed, reactive loop into a predictive, anticipatory one.

### C. Neural Network Architecture

The neural network designed for predicting the homodyne current employs a supervised-learning framework similar to that presented in our earlier work [33], but is trained here on delayed current samples. It consists of an input layer, two hidden layers, and one output layer. Together, these layers allow the network to learn the nonlinear relationship between a short sequence of recent current samples and the next delayed value  $I(t_i+\tau)$ . The hidden layers perform nonlinear transformations that reveal temporal correlations which a simple linear model cannot capture. Figure 5 shows the complete architecture. Each layer is fully connected, every neuron in one layer is connected to every neuron in the next.

- **First hidden layer:** This layer contains 32 neurons. Each neuron receives all five input features from the sliding window of delayed currents  $[I(t_{i-5}+\tau), \dots, I(t_{i-1}+\tau)]$ . Each neuron computes a weighted sum of these inputs, adds a bias, and applies a Rectified Linear Unit (ReLU) activation [34]:

$$h_j^{(1)} = \text{ReLU}\left(\sum_{k=1}^5 w_{jk}^{(1)} x_k + b_j^{(1)}\right), \quad (8)$$

where  $x_k$  is the  $k$ th input feature (current sample),  $w_{jk}^{(1)}$  is the weight connecting feature  $k$  to neuron  $j$ , and  $b_j^{(1)}$

is the bias of that neuron. The ReLU function,

$$\text{ReLU}(z) = \begin{cases} z, & z > 0, \\ 0, & z \leq 0, \end{cases}$$

acts as a nonlinear gate: if the total input  $z$  is positive, the neuron fires and passes the value forward; otherwise it outputs zero. This activation allows the network to learn complex current patterns efficiently without introducing unnecessary computational cost.

- **Second hidden layer:** This layer has 16 neurons, each fully connected to all 32 outputs from the first layer. The operation is again a weighted sum followed by a ReLU activation:

$$h_j^{(2)} = \text{ReLU}\left(\sum_{k=1}^{32} w_{jk}^{(2)} h_k^{(1)} + b_j^{(2)}\right), \quad (9)$$

where  $h_k^{(1)}$  is the activation from neuron  $k$  in the previous layer. This second layer builds higher-level representations that encode correlations between temporal features of the current signal.

- **Output layer:** The final layer consists of a single linear neuron that combines all 16 outputs from the second hidden layer to produce the predicted delayed current:

$$\hat{y}_i = \sum_{j=1}^{16} w_j^{(3)} h_j^{(2)} + b^{(3)} \Rightarrow \hat{y}_i = \hat{I}(t_i+\tau). \quad (10)$$

A linear output (no activation) is used because the homodyne current is a real, unbounded quantity that can take both positive and negative values.

Each neuron therefore performs a simple yet fundamental operation: it takes a weighted sum of its inputs, adds a bias, applies a nonlinear activation (if applicable), and passes the result forward to the next layer. Through many such operations across layers, the network gradually learns to represent the dynamics of the current signal.

*Training objective (MSE loss).*: The supervised learning process adjusts all network parameters  $\theta = \{W, b\}$  to minimize the mean squared error (MSE) between the predicted and true delayed currents:

$$\mathcal{L}_{\text{MSE}}(\theta) = \frac{1}{N} \sum_{i=1}^N [\hat{I}(t_i + \tau) - I(t_i + \tau)]^2. \quad (11)$$

This loss penalizes large deviations and ensures that, on average, the predicted current closely follows the measured delayed current. Training uses the Adam optimizer [35] with mini-batches, standardized inputs, and early stopping based on validation MSE to prevent overfitting.

*Training and prediction phases.*: During the **training phase**, 50% of the delayed dataset is used, where both the inputs  $\mathbf{x}_i$  and the true targets  $y_i$  are known. The network learns by iteratively adjusting its weights to minimize the MSE loss. After convergence—when, for instance,  $\hat{I}(t_5 + \tau) \approx I(t_5 + \tau)$  as in Table I, the model parameters are frozen.

In the **prediction phase**, the remaining 50% of the delayed record is used for testing and live feedback. Here, the trained network receives only the latest five delayed samples and outputs the forecast  $\hat{I}(t_i + \tau)$ , without any access to the true  $I(t_i + \tau)$  value. The controller then applies the predicted current as  $u(t) = \lambda \hat{I}(t + \tau)$ , providing an anticipatory control tone that compensates for the hardware delay. This two-stage process—offline training and online prediction—transforms the feedback loop from reactive to predictive.

Once trained, the neural network effectively acts as a fast, data-driven predictor: it continuously processes new measurements, infers the near-future homodyne current, and drives the feedback controller in advance, thus neutralizing the inherent latency of the experimental loop.

### III. ESTIMATION OF EFFECTIVE LIFETIME AND DECAY RATE

In this section, we describe how the *effective lifetime* and corresponding *decay rate* of the system are extracted under different feedback configurations. Our goal is to quantify how each control strategy, ranging from passive decay to classical, coherent, and predictive feedback, modifies the relaxation dynamics of a two-level system (qubit). The fundamental observable used for this comparison is the excited-state population,

$$P_e(t) \equiv \text{Tr}[\rho(t) \Pi_e], \quad \Pi_e = |e\rangle\langle e|, \quad (12)$$

where  $\rho(t)$  is the system density matrix and  $\Pi_e$  projects onto the excited state  $|e\rangle$ . The trace operation  $\text{Tr}[\cdot]$  ensures that we extract the total probability of finding the system excited at time  $t$ .

For open quantum systems subject to relaxation, the excited-state population typically follows an exponential decay law,

$$P_e(t) = P_e(0) e^{-\Gamma_{\text{eff}} t}, \quad T_1^{\text{eff}} = \Gamma_{\text{eff}}^{-1}, \quad (13)$$

where  $\Gamma_{\text{eff}}$  is the *effective decay rate* and  $T_1^{\text{eff}}$  is the corresponding *effective lifetime*. Eq. 13 defines the performance metrics that we later extract from both numerical simulations and the analytical model. Physically, the smaller  $\Gamma_{\text{eff}}$  (or equivalently, the larger  $T_1^{\text{eff}}$ ), the more effectively the feedback slows the spontaneous emission process.

For a two-level atom or qubit, it is often convenient to use the Pauli-operator basis,  $\sigma_- = |g\rangle\langle e|$ ,  $\sigma_+ = |e\rangle\langle g|$ , and  $\sigma_z = |e\rangle\langle e| - |g\rangle\langle g|$ . In this notation, the standard Lindblad dissipator for any operator  $L$  is

$$\mathcal{D}[L]\rho = L\rho L^\dagger - \frac{1}{2}\{L^\dagger L, \rho\}, \quad (14)$$

where the anticommutator  $\{A, B\} = AB + BA$  guarantees the complete-positivity and trace preservation of the master equation [2], [29].

#### A. No Feedback (Natural Decay)

We begin with the baseline case of spontaneous emission in the absence of any feedback control. In the rotating frame and assuming no external drive, the master equation describing energy relaxation at rate  $\gamma$  reads

$$\dot{\rho} = \gamma \mathcal{D}[\sigma_-]\rho. \quad (15)$$

This equation states that population leaks irreversibly from the excited to the ground state through the jump operator  $\sigma_-$ . To find how the excited-state population evolves, we differentiate Eq. (12) with respect to time and apply the master equation (15):

$$\dot{P}_e(t) = \text{Tr}[\dot{\rho}(t) \Pi_e] = \gamma \text{Tr}[\mathcal{D}[\sigma_-]\rho(t) \Pi_e]. \quad (16)$$

Using standard trace identities (see Appendix A), one obtains

$$\dot{P}_e(t) = -\gamma P_e(t), \quad (17)$$

whose solution is

$$P_e(t) = P_e(0) e^{-\gamma t}, \quad \Gamma_{\text{eff}} = \gamma, \quad T_1 = \gamma^{-1}. \quad (18)$$

Equation (18) thus represents the natural (uncontrolled) exponential decay of a two-level system's excitation, with a relaxation time  $T_1$  equal to the inverse of the spontaneous-emission rate  $\gamma$ .

#### B. Classical (Wiseman–Milburn) Feedback

We next consider the classical continuous-measurement feedback scheme introduced by Wiseman and Milburn [28], [29]. In this setup, a decaying two-level atom emits a fluorescence field that is continuously monitored through homodyne detection. The output field carries information about the system's state, which is converted into a photocurrent  $I(t)$ . This current is then *fed back* to the atom in real time through a control Hamiltonian, with the aim of stabilizing the emission or slowing spontaneous decay. In the ideal Markovian limit, where the loop delay is negligible compared to the system

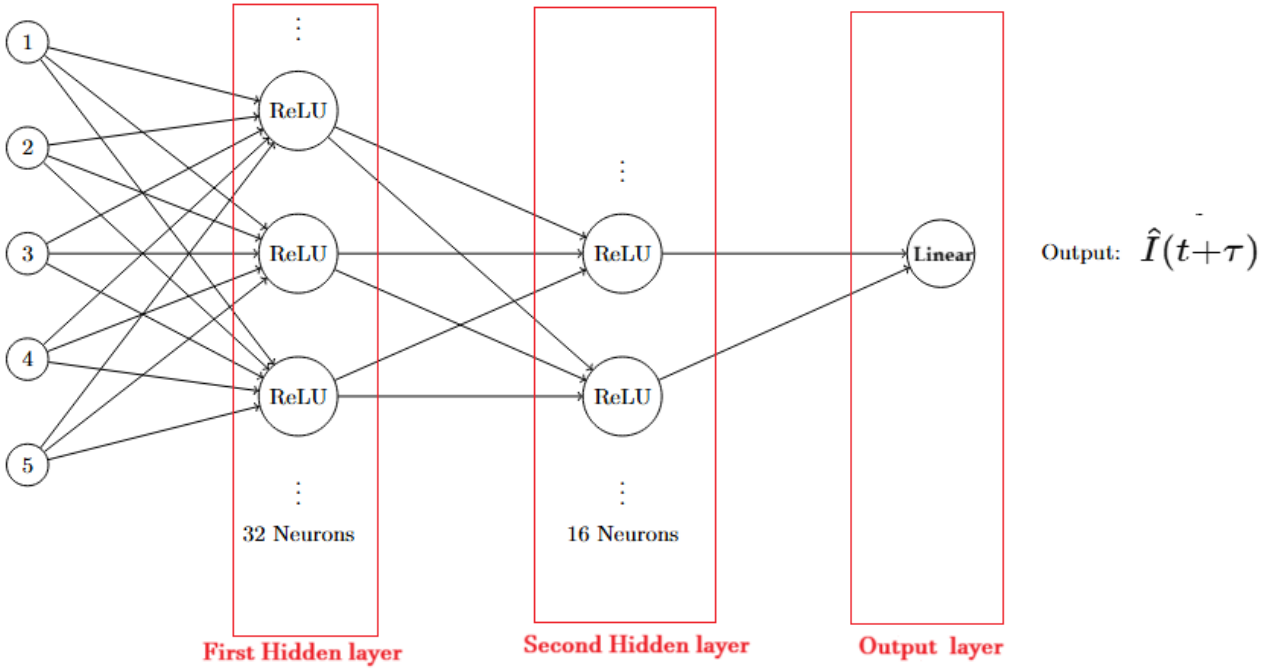


Fig. 5. **Neural network used for homodyne-current prediction.** The input layer receives the last  $W=5$  delayed samples  $[I(t_{i-5}+\tau), \dots, I(t_{i-1}+\tau)]$ . Two hidden layers (32 and 16 neurons) with ReLU activations capture nonlinear dependencies in the time series, and a linear output neuron provides the forecast  $\hat{I}(t_i+\tau)$  used by the controller.

timescale, the unconditional evolution of the atom's density matrix  $\rho(t)$  is governed by the feedback master equation

$$\dot{\rho} = \mathcal{D}[\sqrt{\gamma} \sigma_- - i\lambda \sigma_y] \rho, \quad (19)$$

where  $\gamma$  is the spontaneous-emission rate,  $\lambda$  is the feedback gain, and  $\sigma_y$  is the Pauli operator defining the quadrature on which feedback acts. The Lindblad superoperator  $\mathcal{D}[L]\rho = L\rho L^\dagger - \frac{1}{2}\{L^\dagger L, \rho\}$  captures the irreversible damping caused by photon emission. The additional term  $-i\lambda\sigma_y$  introduces a Hamiltonian correction proportional to the instantaneous measurement record, effectively applying a phase-aligned field that counteracts the decay.

For a two-level system, the excited-state population is directly related to the expectation value of the Pauli operator  $\sigma_z$  through  $P_e(t) = \text{Tr}[\rho(t)\Pi_e] = \frac{1}{2}(1 + \langle\sigma_z\rangle_t)$ , where  $\langle\sigma_z\rangle_t = \text{Tr}[\rho(t)\sigma_z]$ . Differentiating gives  $\dot{P}_e(t) = \frac{1}{2}\frac{d}{dt}\langle\sigma_z\rangle_t$ . Hence, solving for  $\frac{d}{dt}\langle\sigma_z\rangle$  immediately determines how the excited-state population  $P_e(t)$  evolves with time.

*Population equation and effective decay rate.:* Carrying out this derivation (see Appendix B) gives

$$\frac{d}{dt}\langle\sigma_z\rangle = -\Gamma(\lambda) (\langle\sigma_z\rangle + 1), \quad \Gamma(\lambda) = \gamma - 2\sqrt{\eta\gamma}\lambda + 2\lambda^2. \quad (20)$$

Equation (20) clearly shows how feedback modifies the natural decay rate. The first term,  $\gamma$ , represents the intrinsic spontaneous emission. The middle term,  $-2\sqrt{\gamma}\lambda$ , arises from the coherent interference between the emitted field and the applied feedback field: a properly phased feedback current

can partially cancel the emission amplitude, reducing the net decay. The last term,  $+2\lambda^2$ , corresponds to additional decoherence introduced by imperfect or noisy feedback—an unavoidable “price” of driving the atom with a fluctuating current.

*Detection efficiency and optimal feedback gain.:* In realistic experiments, detectors capture only a fraction  $\eta$  of the emitted light. Wiseman and Milburn showed that the feedback strength must therefore be limited to the fraction of information actually measured [28], [29]:

$$\lambda = \frac{1}{2}\sqrt{\eta\gamma}. \quad (21)$$

Substituting this optimal value into Eq. (20) yields the effective decay rate

$$\Gamma_{\text{WM}} = \gamma\left(1 - \frac{\eta}{2}\right), \quad (22)$$

and thus the excited-state population follows

$$P_e(t) = P_e(0)e^{-\Gamma_{\text{WM}}t}, \quad T_1^{\text{WM}} = \frac{1}{\gamma(1 - \eta/2)}. \quad (23)$$

Eq. (22) reveals that the feedback reduces the effective decay rate in direct proportion to the measurement efficiency  $\eta$ . If all the emitted photons are detected ( $\eta = 1$ ), the feedback current carries complete information about the emission process, and the decay rate is halved,  $\Gamma_{\text{WM}} = \gamma/2$ . Consequently, the lifetime doubles,  $T_1^{\text{WM}} = 2/\gamma$ , which is the theoretical limit for any purely classical (measurement-based) feedback. If only half of the emission is captured ( $\eta = 0.5$ ), the lifetime enhancement is modest ( $T_1^{\text{WM}} \approx 1.33/\gamma$ ). This

trade-off emphasizes that the power of classical feedback is fundamentally bounded by how much information can be extracted from the environment: measurement improves control, but incomplete detection leaves residual decoherence. In summary, by working in terms of  $\frac{d}{dt}\langle\sigma_z\rangle$ , we obtain a closed, analytically solvable equation that clearly exposes how feedback gain  $\lambda$  and detection efficiency  $\eta$  renormalize the decay rate. The exponential form of  $P_e(t)$  in Eq. (23) provides a convenient way to extract the effective lifetime  $T_1^{\text{WM}}$  directly from simulation or experiment.

### C. Ancilla-Assisted and Machine-Learning-Enhanced Feedback

While the original W-M feedback loop acts on a single optical quadrature of the emitted field, the next two strategies, *ancilla-assisted* and *machine-learning-enhanced* feedback—introduce additional dynamical resources that further suppress dissipation and extend qubit lifetimes.

(a) *Ancilla-Assisted Feedback*.: In this scheme, the measured homodyne signal is coherently coupled to a secondary two-level system (the *ancilla*) that exchanges excitations with the main qubit. The interaction Hamiltonian is

$$H_{\text{int}} = \hbar g (\sigma_+^{(S)} \sigma_-^{(A)} + \sigma_-^{(S)} \sigma_+^{(A)}), \quad (24)$$

where,  $S$  and  $A$  denote the *system* and *ancilla* qubits, respectively,  $\sigma_{\pm}^{(S/A)}$  are the raising and lowering operators of each qubit,  $g$  is the coherent coupling strength between the two qubits,  $\gamma$  is the intrinsic decay rate of the system qubit.

The ancilla acts as a temporary energy reservoir, coherently exchanging excitations with the system before dissipating them into the environment. When the ancilla relaxes much faster than it couples ( $\kappa \gg g$ ), where  $\kappa$  is the ancilla's spontaneous relaxation rate, it can be *adiabatically eliminated*, yielding an effective decay rate for the system [29], [36]:

$$\Gamma_{\text{anc}} = \frac{\gamma}{1 + C}, \quad C = \frac{4g^2}{\kappa\gamma}, \quad (25)$$

where  $C$  is the *cooperativity parameter*, quantifying how strongly the system–ancilla coupling competes with their dissipation channels. A higher cooperativity  $C$  results in a slower decay, leading to an extended relaxation time

$$T_1^{(\text{anc})} = \frac{1 + C}{\gamma}. \quad (26)$$

(b) *Machine-Learning-Enhanced Feedback (Prediction Only)*.: To mitigate the hardware latency  $\tau$  present in real feedback loops, we introduce a trained neural network that predicts the *future* homodyne current a short time  $\tau$  ahead. The control signal applied to the ancilla is therefore based on this forecast:

$$u_{\text{ML}}(t) = \lambda \hat{I}(t+\tau), \quad (27)$$

where,  $\lambda$  is the scalar feedback gain,  $I(t)$  is the measured (true) homodyne current at time  $t$ ,  $\hat{I}(t+\tau)$  is the predicted current for time  $t + \tau$ , obtained from the most recent delayed samples (Sec. II-B),  $\tau$  is the loop delay arising from analog digital conversion, filtering, and signal routing.

The prediction quality is quantified by the correlation coefficient

$$r = \text{corr}(\hat{I}(t+\tau), I(t+\tau)), \quad 0 \leq r \leq 1, \quad (28)$$

where  $r = 1$  represents perfect anticipation of the true delayed signal, while smaller  $r$  indicates poorer predictive alignment. The residual, uncorrelated noise fraction scales as  $(1 - r^2)$ , which renormalizes the effective decay rate from Eq. (25):

$$\Gamma_{\text{ML}} = \Gamma_{\text{anc}}(1 - r^2) = \frac{\gamma}{1 + C}(1 - r^2). \quad (29)$$

The corresponding lifetime enhancement becomes

$$T_1^{(\text{ML})} = \frac{1 + C}{\gamma(1 - r^2)}. \quad (30)$$

Equation (30) shows that both the coherent coupling ( $C$ ) and the predictive accuracy ( $r$ ) act multiplicatively to extend the qubit lifetime. In the limit of ideal prediction ( $r \rightarrow 1$ ) and strong coupling ( $C \gg 1$ ), the effective relaxation time can greatly exceed the natural  $T_1 = 1/\gamma$ .

For a complete derivation of the effective decay rates  $\Gamma_{\text{anc}}$  and  $\Gamma_{\text{ML}}$  starting from the full system–ancilla master equation, see Appendix C.

## IV. RESULTS AND DISCUSSION

To assess the impact of the three feedback-control architectures, classical Wiseman-Milburn (W-M), ancilla-assisted, and ancilla+ML, we evaluate three complementary observables: the effective lifetime  $T_1$ , the excited-state population  $P_e(t)$ , and the integrated energy-retention function  $E(T)$ . All quantities were computed using IBM-scale parameters: a bare lifetime  $T_1 = 50 \mu\text{s}$ , detection efficiencies  $\eta \in \{0.50, 1.00\}$ , cooperativity  $C = 1.84$ , and correlation coefficient between the predicted and true currents  $r = 0.54$ . The analytical relations for each case are summarized in Table II.

Figure 6 compares the effective lifetimes for all feedback schemes in a bar histogram. Without feedback, the qubit lifetime equals the baseline  $T_1 = 50 \mu\text{s}$ . W-M feedback increases the lifetime depending on the detection efficiency, yielding  $T_1 = 66.7 \mu\text{s}$  for  $\eta = 0.5$  and  $T_1 = 100 \mu\text{s}$  for  $\eta = 1.0$ , corresponding to 1.3x and 2x improvement, respectively. The ancilla-assisted feedback further extends the lifetime to  $142 \mu\text{s}$  ( $C = 1.84$ ), while the ML-assisted variant achieves  $T_1 = 201 \mu\text{s}$ , approximately a fourfold enhancement. The monotonic increase seen in Fig. 5 confirms that adding coherence and prediction progressively improves the system's resistance to relaxation.

Figure 7 presents the time evolution of the excited-state population. Each curve exhibits a single exponential decay characterized by the effective rate in Table II. The uncontrolled system decays most rapidly, followed sequentially by W-M feedback ( $\eta = 0.5$  and  $\eta = 1.0$ ), the ancilla-only case, and finally the ML-enhanced feedback, which shows the slowest decay. At  $t = 100 \mu\text{s}$ , the W-M ( $\eta = 1$ ) population has dropped to about 37%, whereas the ancilla+ML configuration retains approximately 61% of the initial excitation. This clear separation illustrates the predictive scheme's ability to delay

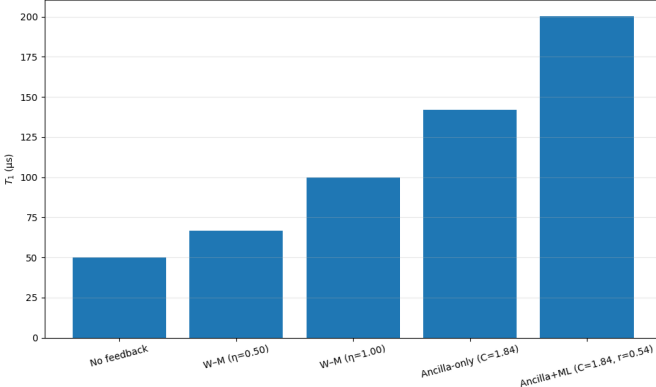


Fig. 6. Effective relaxation times  $T_1$  for the five feedback-control configurations. The baseline (no feedback) corresponds to  $T_1 = 50 \mu\text{s}$ ; W-M feedback improves lifetime by up to  $2\times$ ; ancilla-assisted control extends it to  $142 \mu\text{s}$ ; and the ML-assisted configuration reaches  $T_1 \approx 201 \mu\text{s}$ .

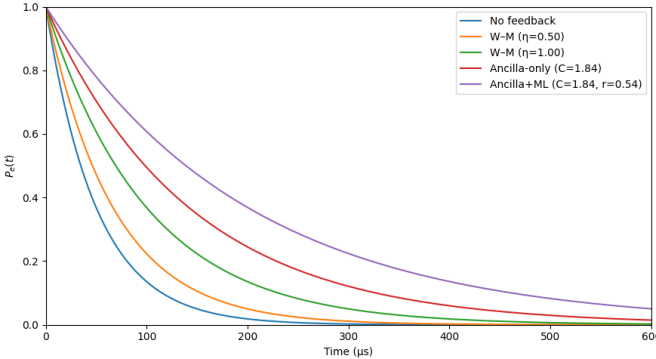


Fig. 7. Time evolution of the excited-state population  $P_e(t)$  under different feedback schemes. The decay slows progressively from the uncontrolled case to W-M, ancilla-only, and finally ancilla+ML, indicating successive suppression of the effective decay rate.

relaxation by compensating for measurement delay and environmental fluctuations.

Figure 8 plots the *energy-retention* curve, defined as the area under the excited-state population up to time  $T$ . Operationally, it is the *cumulative time* the qubit spends excited between 0 and  $T$ . Because the qubit’s internal energy is proportional to its excited-state population, this area is directly proportional to the *total stored energy over the interval*. Equivalently, it quantifies how much excited-state “budget” the controller preserves before that energy is finally emitted into the environment. At short times the curves rise nearly linearly, reflecting that the qubit has not yet had time to relax and the controller is still “banking” energy. As time grows, each curve bends over and approaches a plateau: once almost all excitation has been emitted, accumulating additional “stored energy over time” becomes negligible, so the curve saturates. The height of this plateau is *exactly* the effective lifetime reported in Fig. 6, so the energy-retention plot provides an integral check of the lifetime analysis: higher  $T_1^{(\text{eff})}$  means higher plateau. The saturation level tells us the *total* usable energy preserved by a given control strategy before dissipation wins. Faster

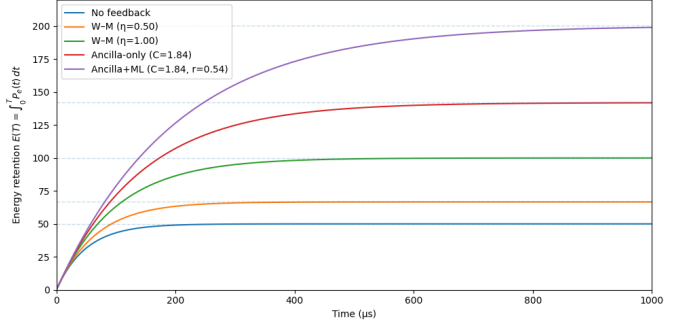


Fig. 8. Energy-retention integral  $E(T)$  versus time for different feedback schemes. Each curve saturates at its effective lifetime  $T_1^{(\text{eff})}$ , validating the lifetime hierarchy observed in Fig. 6. The ancilla+ML configuration exhibits both the highest plateau and the slowest saturation.

saturation means the excited state is depleted quickly (little energy preserved); delayed saturation means the controller keeps the qubit excited for longer, accumulating more stored energy. In our data, no feedback and classical W-M control saturate within  $\sim 200 \mu\text{s}$ , indicating that most of the excitation has been lost by then. Ancilla-assisted control pushes the plateau higher and delays saturation, showing that coherent exchange recycles part of the would-be emission back into the system. With ML prediction, the curve climbs highest and saturates slowest: the controller anticipates the outgoing field, applies a phase-aligned correction, and thereby *maximizes* the time-integrated stored energy. Energy-retention makes the comparison intuitive: it condenses the entire  $P_e(t)$  trajectory into one scalar “area under the curve.” Across all schemes the ordering is consistent with Fig. 5: no feedback  $<$  W-M  $<$  ancilla  $<$  ancilla+ML. In short, strategies that extend the lifetime also deliver the largest retained-energy plateau, and the predictive (ancilla+ML) loop is the most effective at both *slowing* decay and *banking* energy over time.

## V. CONCLUSION

This work presents a coherent pathway to suppress amplitude damping by progressively enriching a measurement–feedback loop with quantum coherence and predictive inference. We benchmarked three architectures, classical Wiseman–Milburn (W-M) feedback, coherent ancilla–assisted feedback, and ancilla feedback augmented with a short-horizon machine-learning (ML) predictor, against natural decay, and evaluated them via effective lifetime, excited-state population decay, and time-integrated energy retention. The closed-form relations used for these comparisons are compiled in Table II.

At the baseline, with no feedback, the qubit relaxes at its natural rate: the lifetime equals the intrinsic  $T_1$ , the population decays accordingly, and the energy-retention integral saturates at  $T_1$ . Classical W-M feedback improves upon this baseline in direct proportion to measurement efficiency, slowing population decay and raising the energy-retention plateau up to the efficiency-limited lifetime. Introducing a coherently coupled ancilla then overcomes the single-quadrature limitation of classical control: by opening a Hamiltonian exchange channel,

it reduces the effective emission rate even without changes to detection, yielding a lifetime increase set by the cooperativity and a commensurate rise in the retained energy. Finally, adding an ML predictor aligns the corrective drive with the *future* emitted field and compensates loop delay, producing the strongest overall improvement: the longest lifetime, the slowest decay, and the highest energy-retention plateau.

These outcomes are mutually consistent: lifetime extension, slower population decay, and increased energy retention move in lockstep because each strategy achieves a further reduction of the effective decay rate. Conceptually, coherence (via the ancilla) recovers information lost in single-quadrature classical feedback, while prediction (via a lightweight supervised model) mitigates unavoidable hardware latency. Practically, the approach is incremental and compatible with standard cavity- and circuit-QED platforms: begin with W-M feedback, add an ancilla path to restore the missing quadrature, and incorporate a short-horizon predictor trained on the homodyne record to anticipate the outgoing field. The resulting gains longer effective lifetimes, reduced decay rates, and larger energy-retention plateaus translate directly into deeper algorithmic circuits and reduced error-correction overheads.

In summary, information that would otherwise be lost to the environment can be captured, processed, and coherently returned to the qubit with the correct phase and timing. In the parameter regimes considered here, classical W-M control improves upon natural decay, ancilla-assisted control provides a further and substantial gain, and the ancilla+ML architecture delivers the largest and most practically relevant enhancement (see Table II).

## REFERENCES

- [1] J. Wang, H. Wiseman, and G. Milburn, “Non-markovian homodyne-mediated feedback on a two-level atom: a quantum trajectory treatment,” *Chemical Physics*, vol. 268, no. 1, pp. 221–235, 2001. [Online]. Available: <https://www.sciencedirect.com/science/article/pii/S0301010401003044>
- [2] H.-P. Breuer and F. Petruccione, *The Theory of Open Quantum Systems*. Oxford University Press, 2002.
- [3] M. A. Nielsen and I. L. Chuang, *Quantum computation and quantum information*. Cambridge University Press, 2010.
- [4] P. Krantz, M. Kjaergaard, F. Yan, T. P. Orlando, S. Gustavsson, and W. D. Oliver, “A quantum engineer’s guide to superconducting qubits,” *Applied Physics Reviews*, vol. 6, no. 2, p. 021318, 2019.
- [5] P. V. Klimov *et al.*, “Optimizing quantum gates towards the scale of logical qubits,” *Nature Communications*, vol. 15, p. 3993, 2024.
- [6] A. G. Fowler, M. Mariantoni, J. M. Martinis, and A. N. Cleland, “Surface codes: Towards practical large-scale quantum computation,” *Physical Review A*, vol. 86, no. 3, p. 032324, 2012.
- [7] E. M. Purcell, “Spontaneous emission probabilities at radio frequencies,” *Physical Review*, vol. 69, p. 681, 1946.
- [8] M. Reagor, H. Paik, G. Catelani, L. Sun, C. Axline, E. T. Holland, I. M. Pop, N. A. Masluk, T. Brecht, L. Frunzio, M. H. Devoret, and R. J. Schoelkopf, “Reaching 10 ms single photon lifetimes for superconducting aluminum cavities,” *Applied Physics Letters*, vol. 102, no. 19, p. 192604, 2013.
- [9] J. Heinsoo, C. K. Andersen, A. Remm, S. Krinner, T. Walter, Y. Salathé, S. Gasparinetti, J.-C. Besse, A. Wallraff, and C. Eichler, “Rapid high-fidelity multiplexed readout of superconducting qubits,” *Physical Review Applied*, vol. 10, no. 3, p. 034040, 2018.
- [10] E. Jeffrey, D. Sank, J. Y. Mutus *et al.*, “Fast accurate state measurement with superconducting qubits,” *Physical Review Letters*, vol. 112, p. 190504, 2014.
- [11] E. A. Sete, J. M. Martinis, and A. N. Korotkov, “Quantum theory of a bandpass purcell filter for qubit readout,” *Physical Review A*, vol. 92, p. 012325, 2015.
- [12] P. A. Spring *et al.*, “Fast multiplexed superconducting-qubit readout with intrinsic tunable purcell filtering,” *PRX Quantum*, vol. 6, p. 020345, 2025.
- [13] E. Yablonovitch, “Inhibited spontaneous emission in solid-state physics and electronics,” *Physical Review Letters*, vol. 58, no. 20, pp. 2059–2062, 1987.
- [14] P. Lodahl, S. Mahmoodian, and S. Stobbe, “Interfacing single photons and single quantum dots with photonic nanostructures,” *Reviews of Modern Physics*, vol. 87, no. 2, pp. 347–400, 2015.
- [15] Ł. Cywiński, R. M. Lutchyn, C. P. Nave, and S. Das Sarma, “How to enhance dephasing time in superconducting qubits,” *Physical Review B*, vol. 77, no. 17, p. 174509, May 2008.
- [16] M. J. Biercuk, H. Uys, A. P. VanDevender, N. Shiga, W. M. Itano, and J. J. Bollinger, “Optimized dynamical decoupling in a model quantum memory,” *Nature*, vol. 458, pp. 996–1000, 2009.
- [17] H. Uys, M. J. Biercuk, and J. J. Bollinger, “Optimized noise filtration through dynamical decoupling,” *Physical Review Letters*, vol. 103, p. 040501, 2009.
- [18] J. Bylander, S. Gustavsson, F. Yan, F. Yoshihara, K. Harrabi, G. Fitch, D. G. Cory, Y. Nakamura, J.-S. Tsai, and W. D. Oliver, “Noise spectroscopy through dynamical decoupling with a superconducting flux qubit,” *Nature Physics*, vol. 7, no. 7, pp. 565–570, Jul. 2011.
- [19] A. Abu-Nada and L.-A. Wu, “Dynamics and control of two coupled quantum oscillators: An analytical approach,” 2025. [Online]. Available: <https://arxiv.org/abs/2509.21492>
- [20] L. Viola and S. Lloyd, “Dynamical decoupling of open quantum systems,” *Physical Review Letters*, vol. 82, pp. 2417–2421, 1999.
- [21] D. A. Lidar, L.-A. Wu, and P. Zanardi, “Decoherence-free subspaces and subsystems,” *Journal of Modern Optics*, vol. 50, no. 6-7, pp. 1047–1057, 2003.
- [22] M. S. Byrd and D. A. Lidar, “Universal dynamical decoupling and quantum error suppression,” *Physical Review A*, vol. 67, p. 012324, 2003.
- [23] L.-A. Wu, M. S. Byrd, and D. A. Lidar, “Efficient dynamical decoupling of multiqubit states,” *Physical Review Letters*, vol. 89, no. 12, p. 127901, 2002.
- [24] N. Ezzell, B. Pokharel, L. Tewala, G. Quiroz, and D. A. Lidar, “Dynamical decoupling for superconducting qubits: A performance survey,” *Physical Review Applied*, vol. 20, no. 6, p. 064027, Dec. 2023.
- [25] A. A. Clerk, M. H. Devoret, S. M. Girvin, F. Marquardt, and R. J. Schoelkopf, “Introduction to quantum noise, measurement, and amplification,” *Reviews of Modern Physics*, vol. 82, no. 2, pp. 1155–1208, Jun. 2010.
- [26] G. Ithier, E. Collin, P. Joyez, P. J. Meeson, D. Vion, D. Esteve, F. Chiarello, A. Shnirman, Y. Makhlin, J. Schrieffl, and G. Schön, “Decoherence in a superconducting quantum bit circuit,” *Physical Review B*, vol. 72, no. 13, p. 134519, Oct. 2005.
- [27] T. J. Green, J. Sastrawan, H. Uys, and M. J. Biercuk, “Dynamical decoupling sequence construction as a filter-design problem,” *New Journal of Physics*, vol. 15, p. 095004, 2013.
- [28] H. M. Wiseman and G. J. Milburn, “Quantum theory of optical feedback via homodyne detection,” *Physical Review Letters*, vol. 70, no. 5, pp. 548–551, 1993.
- [29] ———, *Quantum Measurement and Control*. Cambridge University Press, 2009.
- [30] A. C. Doherty and K. Jacobs, “Quantum feedback control and classical control theory,” *Physical Review A*, vol. 60, no. 4, pp. 2700–2711, 1999.
- [31] H. J. Carmichael, *An Open Systems Approach to Quantum Optics*, ser. Lecture Notes in Physics Monographs. Springer, 1993.
- [32] K. Jacobs and D. A. Steck, “A straightforward introduction to continuous quantum measurement,” *Contemporary Physics*, vol. 47, no. 5, pp. 279–303, 2006.
- [33] A. Abu-Nada and S. Banerjee, “Supervised machine learning for predicting open quantum system dynamics and detecting non-markovian memory effects,” 2025. [Online]. Available: <https://arxiv.org/abs/2509.22758>
- [34] V. Nair and G. E. Hinton, “Rectified linear units improve restricted boltzmann machines,” in *Proceedings of the 27th International Conference on Machine Learning (ICML-10)*, 2010, pp. 807–814.
- [35] D. P. Kingma and J. Ba, “Adam: A method for stochastic optimization,” *arXiv preprint arXiv:1412.6980*, 2014.

TABLE II

COMPARISON OF FEEDBACK SCHEMES FOR AMPLITUDE-DAMPING SUPPRESSION. HERE  $P_e(t)$  IS THE EXCITED-STATE POPULATION,  $\Gamma_{\text{eff}}$  THE EFFECTIVE DECAY RATE, AND  $T_1^{\text{eff}} = 1/\Gamma_{\text{eff}}$  THE CORRESPONDING LIFETIME.

Scheme	$P_e(t)$	$\Gamma_{\text{eff}}$	$T_1^{\text{eff}}$
No feedback	$P_e(0) e^{-\gamma t}$	$\gamma$	$1/\gamma$
W-M (optimal, efficiency $\eta$ )	$P_e(0) e^{-\gamma(1-\eta/2)t}$	$\gamma(1-\eta/2)$	$1/[\gamma(1-\eta/2)]$
Ancilla-only (cooperativity $C = 4g^2/(\kappa\gamma)$ )	$P_e(0) e^{-\frac{\gamma}{1+C}t}$	$\gamma/(1+C)$	$(1+C)/\gamma$
Ancilla + ML (prediction quality $r = \text{corr}(\hat{I}, I)$ )	$P_e(0) e^{-\frac{\gamma}{1+C}(1-r^2)t}$	$\frac{\gamma}{1+C}(1-r^2)$	$\frac{1+C}{\gamma(1-r^2)}$

[36] J. E. Gough, “Quantum feedback networks: modelling and synthesis,” *Proceedings of the Royal Society A*, vol. 468, no. 2146, p. 2189–2204, 2010.

## APPENDIX A DERIVATION OF EQ. (17)

Starting from the master equation with spontaneous emission at rate  $\gamma$ ,

$$\dot{\rho}(t) = \gamma \mathcal{D}[\sigma_-]\rho(t) = \gamma(\sigma_- \rho \sigma_+ - \frac{1}{2}\{\sigma_+ \sigma_-, \rho\}), \quad (31)$$

where the Lindblad dissipator is defined as

$$\mathcal{D}[L]\rho = L\rho L^\dagger - \frac{1}{2}\{L^\dagger L, \rho\}, \quad (32)$$

where  $\{X, Y\} = XY + YX$  denotes the anticommutator. This equation describes the irreversible loss of excitation from the upper state  $|e\rangle$  to the ground state  $|g\rangle$ .

The excited-state population is defined by

$$P_e(t) = \text{Tr}[\rho(t)\Pi_e], \quad \Pi_e = |e\rangle\langle e|. \quad (33)$$

Differentiating and using linearity of the trace gives

$$\dot{P}_e(t) = \text{Tr}[\dot{\rho}(t)\Pi_e] = \gamma \text{Tr}[\mathcal{D}[\sigma_-]\rho(t)\Pi_e]. \quad (34)$$

Expanding the dissipator and applying the cyclic property  $\text{Tr}[AB] = \text{Tr}[BA]$ ,

$$\begin{aligned} \text{Tr}[\mathcal{D}[\sigma_-]\rho\Pi_e] &= \text{Tr}[\sigma_- \rho \sigma_+ \Pi_e] - \frac{1}{2} \text{Tr}[(\sigma_+ \sigma_-) \rho \Pi_e] \\ &\quad - \frac{1}{2} \text{Tr}[\rho(\sigma_+ \sigma_-) \Pi_e]. \end{aligned} \quad (35)$$

For a two-level atom  $\sigma_- = |g\rangle\langle e|$ ,  $\sigma_+ = |e\rangle\langle g|$ ,  $\sigma_+ \sigma_- = \Pi_e$ , and  $\Pi_e \sigma_- = 0$ ,  $\sigma_+ \Pi_e = 0$ . Hence the first term vanishes,  $\text{Tr}[\sigma_- \rho \sigma_+ \Pi_e] = 0$ , and the remaining two yield

$$-\frac{1}{2} \text{Tr}[\Pi_e \rho \Pi_e] - \frac{1}{2} \text{Tr}[\rho \Pi_e] = -\text{Tr}[\rho \Pi_e] = -P_e(t), \quad (36)$$

where  $\Pi_e^2 = \Pi_e$  has been used. Therefore,

$$\dot{P}_e(t) = -\gamma P_e(t), \quad P_e(t) = P_e(0) e^{-\gamma t}, \quad (37)$$

so that the effective decay rate is  $\Gamma_{\text{eff}} = \gamma$  and the lifetime  $T_1 = \gamma^{-1}$ .

## APPENDIX B DERIVATION OF THE WISEMAN–MILBURN FEEDBACK EQUATION

Because the excited-state probability is related to the population-difference operator by

$$P_e = \frac{1}{2}(1 + \langle \sigma_z \rangle), \quad (38)$$

its time derivative is directly determined by the evolution of  $\langle \sigma_z \rangle$ . In this appendix we show that feedback modifies the decay to

$$\dot{P}_e = -\Gamma(\lambda, \eta) P_e, \quad P_e(t) = P_e(0) e^{-\Gamma(\lambda, \eta)t}, \quad (39)$$

with an effective rate  $\Gamma(\lambda, \eta)$  that depends on the feedback gain  $\lambda$  and the detection efficiency  $\eta$ . To obtain this result we first derive  $d\langle \sigma_z \rangle/dt$  from the Wiseman-Milburn master equation.

In the W-M feedback scheme, the detector measures the light emitted by the atom and immediately applies a feedback signal back to the atom. If the homodyne detector is not perfect, only a fraction of the emitted light is detected. We describe the detector efficiency by a number  $0 \leq \eta \leq 1$ , where  $\eta = 1$  represents perfect detection and  $\eta = 0$  means no detection at all.

The unconditional master equation for the system’s density matrix  $\rho$  is

$$\dot{\rho} = \mathcal{D}[c - i\sqrt{\eta}F]\rho + (1 - \eta)\mathcal{D}[F]\rho, \quad (40)$$

where,  $c = \sqrt{\gamma}\sigma_-$ ,  $F = \lambda\sigma_y$ ,  $\gamma$  is the natural decay rate,  $\lambda$  is the feedback strength,  $\sigma_- = |g\rangle\langle e|$  is the lowering operator, and  $\sigma_y$  is the Pauli  $y$  matrix.

In experiments we do not directly observe  $\rho$ ; instead we measure expectation values  $\langle A \rangle = \text{Tr}(A\rho)$  of physical observables  $A$ . To find their time evolution we differentiate:

$$\frac{d}{dt}\langle A \rangle = \frac{d}{dt}\text{Tr}(A\rho) = \text{Tr}(A\dot{\rho}). \quad (41)$$

Substituting Eq. (40) for  $\dot{\rho}$  gives

$$\frac{d}{dt}\langle A \rangle = \text{Tr}(A\mathcal{D}[c - i\sqrt{\eta}F]\rho) + (1 - \eta)\text{Tr}(A\mathcal{D}[F]\rho). \quad (42)$$

It is often more convenient to let the dissipator act on  $A$  instead of on  $\rho$ . For any operator  $L$  we therefore define the *adjoint dissipator*

$$\mathcal{D}^\dagger[L]A = L^\dagger AL - \frac{1}{2}\{L^\dagger L, A\}, \quad (43)$$

which satisfies the trace identity

$$\mathrm{Tr}(A \mathcal{D}[L]\rho) = \mathrm{Tr}(\mathcal{D}^\dagger[L]A\rho). \quad (44)$$

Using this in Eq. (42) gives the compact and general formula

$$\frac{d}{dt}\langle A \rangle = \mathrm{Tr}[\mathcal{D}^\dagger[c - i\sqrt{\eta}F]A\rho] + (1-\eta)\mathrm{Tr}[\mathcal{D}^\dagger[F]A\rho]. \quad (45)$$

This relation is crucial: it connects the master equation for  $\rho$  with the measurable time evolution of any observable  $A$ .

To study population dynamics we now set  $A = \sigma_z$ , the population-difference operator, and use the Pauli-matrix relations

$$\begin{aligned} \sigma_\pm &= \frac{1}{2}(\sigma_x \pm i\sigma_y), & \sigma_+\sigma_- &= \frac{1}{2}(I + \sigma_z), \\ \sigma_-\sigma_+ &= \frac{1}{2}(I - \sigma_z), & \sigma_y^2 &= I, \\ \sigma_y\sigma_z &= -\sigma_z\sigma_y = 2i(\sigma_+ - \sigma_-). \end{aligned}$$

After substituting  $c = \sqrt{\gamma}\sigma_-$  and  $F = \lambda\sigma_y$ , and expanding the commutators step by step, one finds

$$\mathcal{D}^\dagger[c - i\sqrt{\eta}F]\sigma_z = -(\gamma - 2\sqrt{\eta\gamma}\lambda + 2\lambda^2)(\sigma_z + I), \quad (46)$$

$$\mathcal{D}^\dagger[F]\sigma_z = -2\lambda^2\sigma_z. \quad (47)$$

Substituting these into Eq. (45) and simplifying yields

$$\frac{d}{dt}\langle\sigma_z\rangle = -\Gamma(\lambda, \eta)(\langle\sigma_z\rangle + 1), \quad \Gamma(\lambda, \eta) = \gamma - 2\sqrt{\eta\gamma}\lambda + 2\lambda^2. \quad (48)$$

Combining Eq. (48) with the relation (38) immediately gives

$$\dot{P}_e = -\Gamma(\lambda, \eta)P_e, \quad P_e(t) = P_e(0)e^{-\Gamma(\lambda, \eta)t},$$

which is Eq. (39).

Minimizing  $\Gamma(\lambda, \eta)$  with respect to  $\lambda$  gives the optimal feedback strength

$$\frac{d\Gamma}{d\lambda} = -2\sqrt{\eta\gamma} + 4\lambda = 0 \quad \Rightarrow \quad \lambda^* = \frac{1}{2}\sqrt{\eta\gamma},$$

and since  $d^2\Gamma/d\lambda^2 = 4 > 0$  this is indeed a minimum. At this optimum,

$$\Gamma_{\mathrm{WM}} = \Gamma(\lambda^*, \eta) = \gamma\left(1 - \frac{\eta}{2}\right), \quad (49)$$

$$T_1^{\mathrm{WM}} = \frac{1}{\Gamma_{\mathrm{WM}}} = \frac{1}{\gamma(1 - \eta/2)}. \quad (50)$$

For perfect detection ( $\eta = 1$ ),  $\Gamma_{\mathrm{WM}} = \gamma/2$  and  $T_1^{\mathrm{WM}} = 2/\gamma$ , so the feedback doubles the lifetime of the excited state. For inefficient detection ( $\eta < 1$ ), the improvement is smaller because less information is available to the feedback loop.

W-M feedback can slow down spontaneous emission by an amount that depends directly on the detection efficiency  $\eta$ . The better the detection, the more the feedback can suppress decay, and in the ideal limit of  $\eta = 1$ , the lifetime doubles compared with natural spontaneous emission.

## APPENDIX C

### DERIVATION OF THE ANCILLA AND ML FEEDBACK RATES

This Appendix presents a detailed, step-by-step derivation of the effective decay rates  $\Gamma_{\mathrm{anc}}$  and  $\Gamma_{\mathrm{ML}}$  corresponding to the ancilla-assisted and machine-learning-enhanced feedback schemes. Our aim is to make transparent how coupling a fast-decaying ancilla qubit to a more slowly relaxing system qubit, together with predictive feedback, leads to a net suppression of the system's relaxation rate.

#### A. Joint Master Equation

We consider a system qubit  $S$  coupled to an ancilla qubit  $A$  with joint density matrix  $\rho_{SA}$ . Their full dynamics are governed by

$$\begin{aligned} \dot{\rho}_{SA} = & -\frac{i}{\hbar}[H_S + H_A + H_{\mathrm{int}}, \rho_{SA}] + \gamma \mathcal{D}[\sigma_-^{(S)}]\rho_{SA} \\ & + \kappa \mathcal{D}[\sigma_-^{(A)}]\rho_{SA}, \end{aligned} \quad (51)$$

where,  $\mathcal{D}[L]\rho = L\rho L^\dagger - \frac{1}{2}(L^\dagger L\rho + \rho L^\dagger L)$ , is the Lindblad dissipator,  $\gamma$  is the spontaneous-emission rate of the system, and  $\kappa$  is the relaxation rate of the ancilla.

The two qubits exchange excitations through the Hamiltonian

$$H_{\mathrm{int}} = \hbar g(\sigma_+^{(S)}\sigma_-^{(A)} + \sigma_-^{(S)}\sigma_+^{(A)}), \quad (52)$$

where  $g$  is the coherent coupling strength.

We will assume the fast-ancilla regime  $\kappa \gg g, \gamma$ , so the ancilla reacts almost instantly to changes in the system.

#### B. Factorization and Weak-Coupling Approximation

The total state can always be written as  $\rho_{SA} = \rho_S \otimes \rho_A + \chi$ , where  $\chi$  represents the correlations between the two qubits. Because  $g$  is small, these correlations are weak ( $\chi \sim O(g)$ ). Keeping only first-order terms in  $g$  corresponds to the Born or weak-coupling approximation:

$$\rho_{SA} \approx \rho_S \otimes \rho_A. \quad (53)$$

With this simplification, the reduced equations of motion become

$$\dot{\rho}_S = -\frac{i}{\hbar}\mathrm{Tr}_A[H_{\mathrm{int}}, \rho_S \otimes \rho_A] + \gamma \mathcal{D}[\sigma_-^{(S)}]\rho_S, \quad (54)$$

$$\dot{\rho}_A = -\frac{i}{\hbar}\mathrm{Tr}_S[H_{\mathrm{int}}, \rho_S \otimes \rho_A] + \kappa \mathcal{D}[\sigma_-^{(A)}]\rho_A. \quad (55)$$

These two equations are treated consistently. The system evolves slowly, while the ancilla reaches a quasi-steady state that we can solve for and then substitute back.

#### C. Ancilla Dynamics and Adiabatic Elimination

The purpose of this step is to find how the ancilla responds to the system.

*Step 1: Equation of motion for  $\langle \sigma_-^{(A)} \rangle$ :* Taking the trace of Eq. (55) with  $\sigma_-^{(A)}$  yields

$$\begin{aligned} \frac{d}{dt} \langle \sigma_-^{(A)} \rangle &= -\frac{i}{\hbar} \text{Tr}_{S,A} [\sigma_-^{(A)} [H_{\text{int}}, \rho_S \otimes \rho_A]] \\ &+ \kappa \text{Tr}_A [\sigma_-^{(A)} \mathcal{D}[\sigma_-^{(A)}] \rho_A]. \end{aligned} \quad (56)$$

The first trace runs over both the system ( $S$ ) and the ancilla ( $A$ ) because the interaction Hamiltonian  $H_{\text{int}}$  couples the two subsystems; hence, evaluating the expectation value requires summing over their joint Hilbert space. In contrast, the second term involves the local dissipator  $\mathcal{D}[\sigma_-^{(A)}]$ , which acts only on the ancilla, so the trace is taken solely over the ancilla subspace.

*Step 2: Evaluate each part:* From the Hamiltonian in Eq. (52) and basic Pauli algebra,

$$\text{Tr}_{S,A} [\sigma_-^{(A)} [H_{\text{int}}, \rho_S \otimes \rho_A]] = \hbar g i \langle \sigma_-^{(S)} \sigma_z^{(A)} \rangle.$$

The dissipator contributes the standard damping term  $-(\kappa/2) \langle \sigma_-^{(A)} \rangle$ . Thus,

$$\frac{d}{dt} \langle \sigma_-^{(A)} \rangle = -\frac{\kappa}{2} \langle \sigma_-^{(A)} \rangle - ig \langle \sigma_-^{(S)} \sigma_z^{(A)} \rangle. \quad (57)$$

*Step 3: Ground-state approximation:* Because the ancilla spends most of the time in its ground state,  $\langle \sigma_z^{(A)} \rangle \approx -1$ . Replacing this in Eq. (57) gives

$$\frac{d}{dt} \langle \sigma_-^{(A)} \rangle \approx -\frac{\kappa}{2} \langle \sigma_-^{(A)} \rangle + ig \langle \sigma_-^{(S)} \rangle.$$

*Step 4: Adiabatic (steady-state) limit:* Since  $\kappa$  is very large, the ancilla follows the system almost instantaneously. Setting the derivative to zero ( $\langle \sigma_-^{(A)} \rangle \approx 0$ ) yields the steady-state solution

$$\langle \sigma_-^{(A)} \rangle \approx \frac{2ig}{\kappa} \langle \sigma_-^{(S)} \rangle. \quad (58)$$

This result means the ancilla coherence is always proportional to the system coherence, but smaller by a factor  $2g/\kappa$ . At the operator level we write  $\sigma_-^{(A)} \simeq \frac{2ig}{\kappa} \sigma_-^{(S)}$ .

#### D. Ancilla-Induced Dissipation and Cooperativity

We now ask: if the ancilla approximately follows the relation  $\sigma_-^{(A)} \simeq (2ig/\kappa) \sigma_-^{(S)}$ , how does this influence the system's decay dynamics?

*Step 5: Substituting into the ancilla dissipator:* The ancilla's decay term in Eq. (51) is given by  $\kappa \mathcal{D}[\sigma_-^{(A)}] \rho_{SA}$ . Replacing  $\sigma_-^{(A)}$  by its approximate expression in terms of  $\sigma_-^{(S)}$  yields

$$\kappa \mathcal{D}[\sigma_-^{(A)}] \rho_{SA} \simeq \frac{4g^2}{\kappa} \mathcal{D}[\sigma_-^{(S)}] \rho_{SA}.$$

Taking the partial trace over the ancilla ( $\text{Tr}_A \rho_{SA} = \rho_S$ ) means tracing out the ancilla degrees of freedom from the *total joint master equation* (Eq. (51)), which governs the full system-ancilla dynamics. This operation leaves only the system's reduced dynamics and leads to

$$\dot{\rho}_S = \left( \gamma + \frac{4g^2}{\kappa} \right) \mathcal{D}[\sigma_-^{(S)}] \rho_S. \quad (59)$$

This shows that the system experiences an additional dissipation channel mediated by its coupling to the ancilla.

*Step 6: Defining the cooperativity:* To make the result more intuitive, we compare the coherent coupling strength  $g$  with the system's intrinsic decay rate  $\gamma$  and the ancilla's damping rate  $\kappa$ . This motivates the definition of the **cooperativity parameter**:

$$C = \frac{4g^2}{\kappa\gamma}. \quad (60)$$

Physically,  $C$  quantifies how effectively an excitation can cycle between the system and the ancilla before being lost. A larger  $C$  indicates stronger recycling and hence slower overall decay of the system.

Rewriting Eq. (59) in terms of  $C$  gives a compact expression for the *effective decay rate*:

$$\Gamma_{\text{anc}} = \frac{\gamma}{1 + C}. \quad (61)$$

The corresponding relaxation time is therefore

$$T_1^{(\text{anc})} = \frac{1 + C}{\gamma}.$$

#### E. Inclusion of ML Predictive Feedback

We now include the machine-learning (ML) prediction used to drive the ancilla based on a forecast of the homodyne current.

The ML controller generates a predicted signal  $\hat{I}(t + \tau)$  a short time  $\tau$  ahead. The ancilla drive is  $u_{\text{ML}}(t) = \lambda \hat{I}(t + \tau)$ , where  $\lambda$  is a gain constant.

The prediction quality is quantified by the correlation coefficient

$$r = \text{corr}(\hat{I}(t + \tau), I(t + \tau)), \quad 0 \leq r \leq 1. \quad (62)$$

Here  $r = 1$  means perfect prediction and  $r = 0$  means no predictive power. The remaining uncorrelated noise has variance proportional to  $(1 - r^2)$ .

This noise reduces the feedback efficiency. Mathematically we include it by rescaling the system collapse operator as

$$\sigma_-^{(S)} \rightarrow (1 - r^2)^{1/2} \sigma_-^{(S)}. \quad (63)$$

Substituting this into the ancilla-modified equation gives

$$\Gamma_{\text{ML}} = \Gamma_{\text{anc}} (1 - r^2) = \frac{\gamma}{1 + C} (1 - r^2). \quad (64)$$

The corresponding lifetime is

$$T_1^{(\text{ML})} = \frac{1 + C}{\gamma (1 - r^2)}. \quad (65)$$